RICE UNIVERSITY

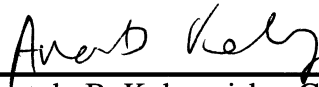# Cooperative mechanisms in coupled motor proteins transport

by
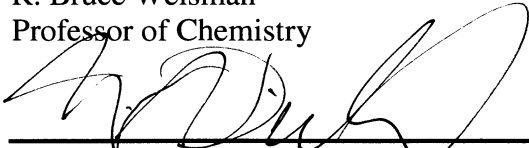
Karthik Uppulury

A THESIS SUBMITTED
IN PARTIAL FULFILLMENT OF THE
REQUIREMENTS FOR THE DEGREE

Master of Arts

APPROVED, THESIS COMMITTEE

Anatoly B. Kolomeisky, Chair
Professor of Chemistry

R. Bruce Weisman
Professor of Chemistry

Michael R. Diehl
Assistant Professor of Bioengineering

Junrong Zheng
Assistant Professor of Chemistry

HOUSTON, TEXAS
November 2011

Abstract

Cooperative mechanisms in coupled motor proteins transport

by

Karthik Uppulury

Subcellular cargos are transported by enzyme molecules called molecular motors by using the chemical energy from hydrolysis of ATP and performing mechanical work in non-equilibrium. Certain motors tread on cytoskeleton structures i.e microtubules and actin filaments in a linear manner. Due to the polarity of the cytoskeleton structures the motors can accomplish cellular transport along one direction. Cargos often rely upon the collective action of more than one motor to transport them in order to surmount the crowding and visco-elastic effects of the surrounding medium through higher force generation. To understand the mechanism of cargo transport by precisely two kinesin-1 motors a combination of experimental and theoretical approaches were employed. This thesis focuses on understanding the mechanism of transport by considering interactions between closely spaced motors on the microtubules. The main finding of this thesis is that motors under the influence of each other's interaction with microtubules do affect the cargo dynamics.

Acknowledgments

I would like to thank my adviser Dr. Anatoly B. Kolomesiky for introducing me to the field of molecular motors and for having allowed me to work on my master's thesis in his group which would have not been possible without his support and encouragement. I would like to thank our collaborator Dr. Michael R. Diehl for the scientific discussions towards a quantitative understanding of the measurements performed at the Diehl lab. I would like to thank my parents for their constant support.

Contents

List of figures

List of Equations

Chapter 1

Multiple Motors Transport

Molecular motors are active enzyme molecules that utilize the available chemical energy to perform mechanical work in non-equilibrium, isothermal conditions. They harness this energy through hydrolysis of ATP or related energy rich compounds. Motor proteins can be classified based on their functional properties.[1,2] Important classes of motors perform rotational motion to synthesize ATP inside mitochondria, such as F_0F_1-ATPase and bacterial flagella motors.[3,4,5,6] Several other classes of motors tread on cytoskeleton structures like microtubules and actin in a linear manner and could be to referred to as translocases. Motors belonging to kinesin, dynein and myosin super family are translocases. These cytoskeleton structures are composed of individual sub-units which have an inherent polarity, due to which a net direction of motion can be assigned for motion of the motors on the macroscopic structures and transport in one direction.[1,7-14] Cellular components such as vesicles and peroxisomes are transported by motors from one destination site to another under controlled spatio-temporal conditions by the action of motors.[15-17,42]

Employing state-of-the art technologies that can control motions of individual motor protein molecules, significant progress has been achieved in understanding

the underlying mechanisms of motor proteins transport.[18-24] The growing experimental evidences offer new insights into motor cooperativity and regulation of cargos.[27-33] Theoretical models are much needed for a comprehensive and concrete quantitative understanding and predictive power.[34-39]

Cellular cargos are acted upon by multiple motors to surmount the challenge of higher force production for transport due to crowding effects and visco-elastic properties of the surrounding medium. Cargos can also be regulated by a team of motors acting on it. However, much is not known about the underlying mechanisms of transport in such scenarios. The Optical tweezers are a useful tool to probe system dynamics involving cargo transport by motors. The technology enables one to apply measurable forces of the order of pico-Newton on a system of interest.[25,26] In the earlier study of multiple motors system the influence of myosin-V and kinesin on each other's processive abilities pertinent to cargo transport was studied.[40] In another study Dietz *et al* studied collective dynamics of multiple motor systems (two and three) in an upside down gliding assay where MT's are the cargo and kinesin motors were bound to an immovable surface.[41]

A more biologically relevant *in-vitro* set up for multiple motor dynamics was engineered by Diehl lab which allowed studies on cargo transport by precisely two motors to be performed.[45] Employing optical trapping techniques the measurements were conducted and a quantitative model was developed for a concrete understanding of the same. One of the key findings of two kinesin-1 cargo transport is that the motors cooperate negatively below the stalling force of kinesin-

1 motor and cooperative effects are noted when the collective force acting on the motors is higher than the stalling force of the kinesin-1 motor.[46,48]   The work presented in this thesis is based on *in-vitro* studies pertinent to two kinesin-1 based transport and addresses the issue of motor cooperation at high forces. A mechanism at the molecular level is probed to explain the measured trend of cargo velocities under different experimental set ups (static optical trap and force feedback). A generalized model is proposed that considers interactions between motors when they are closely spaced on the microtubules into consideration to calculate the dynamical properties of the system. Our model successfully explains the observed behavior of high cargo velocities under higher applied loads in the experiments.

Chapter 2

Coupled motors system and their dynamic properties – an *in-vitro* study

The system of interest is a cargo molecule (a polystyrene bead) conjugated to a two kinesin-1 assembly (Fig 2.1) that transports the bead along the microtubule. Initially the bead is trapped by focusing a laser beam onto it. The motors, in a saturated ATP medium, exert forces on the cargo and pull the cargo away from the center of the trap along the direction of the motor stepping.
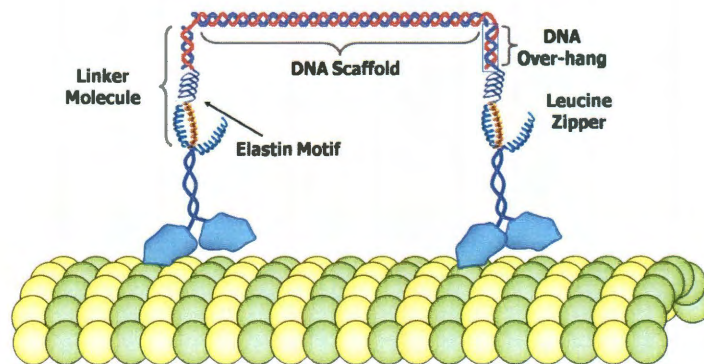

Figure 2.1- A two kinesin-1 bio-synthetic assembly.
The assembly comprises of two human kinesin-1 motor constructs connected by a DNA scaffold (50 nm) via a linker molecule. Taken from: Rogers *et al*, PCCP 11, 4882, 2009.

The motors perform mechanical work by generating force on the cargo when the motor takes a step forward. The forces that the motors exert on the cargos are

dependent on the motor's elastic stretching properties under applied loads. As a result of the forces acting on the bead and it's displacement from the focus of the trap, a restoring force acts on the bead towards the focus of the trap. This force arises due to the change in the momentum of the refracted photons from the bead when it is displaced from the center of the trap since the laser beam basically uses a non-uniform intensity profile with the brightest light being at the focus of the trap (Fig 2.2).
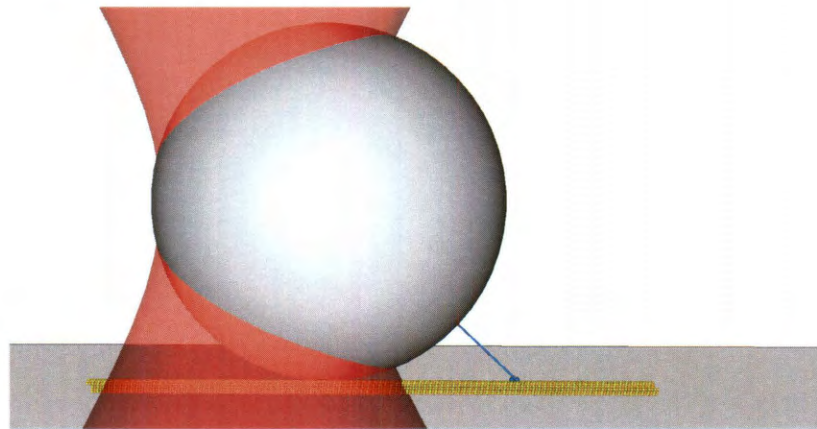
Figure 2.2 – Kinesin-1cargo complex in a static optical trap
Schematic of a polystyrene bead acted upon by a motor moving on the microtubule, whilst the bead trapped by the laser beam. Taken from: Jamison *et al,* Biophysical Journal 99, 2967, 2010.

The trace of a single motor cargo complex in a static optical trap is depicted in (Fig 2.3) shows the motion of the bead in the trap. The force gradually increases on the bead due to motor's forward steps on the microtubule, and under increasing

loads the motor's velocity decreases to zero when the force on the motor builds up to approximately 7 pico-Newton and thereby detaches from the microtubule. The red dotted line corresponds to the stalling force of a single kinesin-1 motor. The trace of a two motor cargo complex evinces higher force production i.e forces above that of single kinesin-1 stall force which serves as one of the first evidences for collective action of kinesin-1 on cargos.
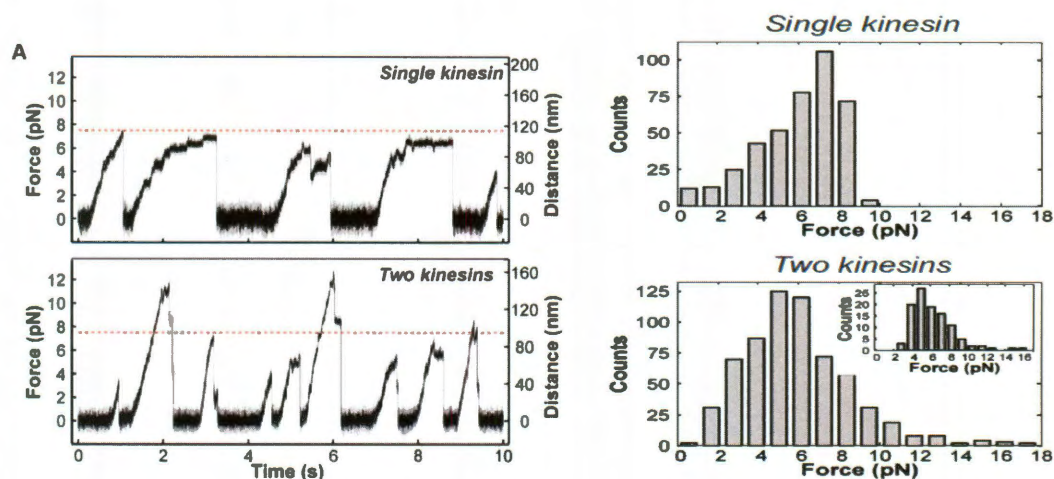
Figure 2.3 – Traces and peak force distributions.
On the left, trace of a single kinesin system (top) and two kinesin system (bottom) are shown. On the right, peak force distributions of single kinesin system (top) and two kinesin system (bottom) are shown. The peak force distribution in the inset corresponds to one particular bead. Taken from: Jamison *et al*, Biophysical Journal 99, 2967, 2010.

The histogram distributions in (Fig 2.3) represent peak forces that develop on the bead in a static optical trap before the bead detaches from the microtubule during that run. The peak force distribution for the single motor complex has a peak

distributed around approx 7.6 pN. The peak force distribution of the two motors complex resembles that of the single motor complex below the single motor stall force and so the two kinesin-1motors can collectively generate higher forces but most often they behave like a single kinesin-1 system. The other evidences for two motor bound configurations are two state detachment process, bi-modal velocities of cargo, higher stiffness of the two kinesin-1 assembly compared to single motor stiffness and attenuated cargo size displacements of the cargo. A two state detachment process is depicted in (Fig 2.4) in which a two motor bound state represented by '**1**' retracts back to the focus of the trap via a single motor bound configuration '**2**'. The bead velocities under an applied load of 5 pN shows a behavior that is single motor like and two motor like with distinct distributions in their velocities. The stiffness of the composite system is higher compared to the stiffness of the single motor case which signifies the presence of two motor bound configurations.
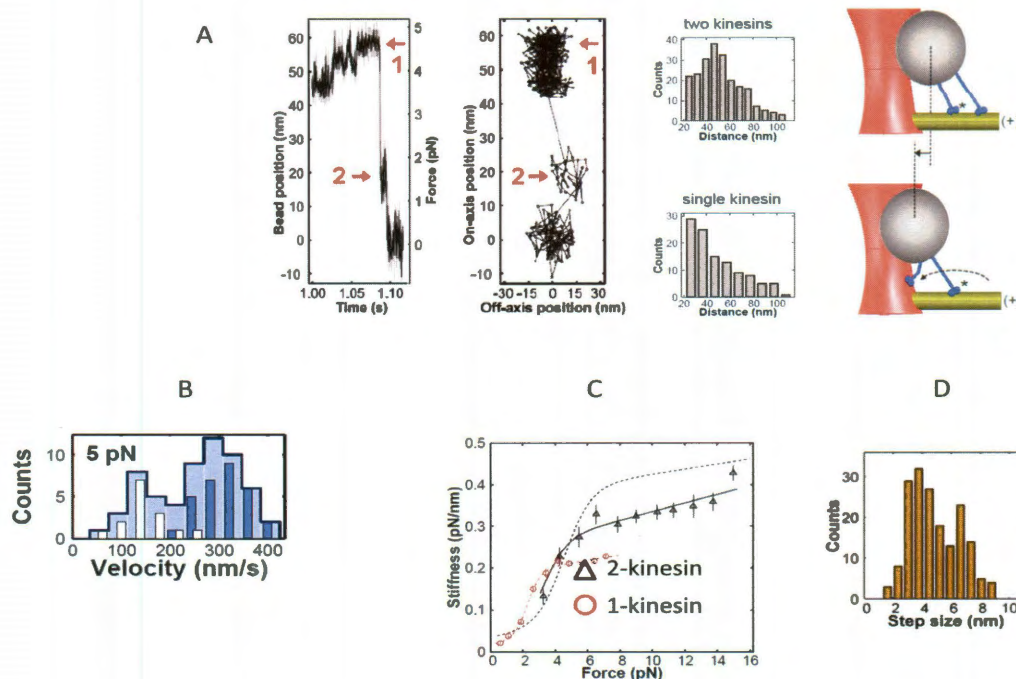
Figure 2.4 – Signatures of two motor states.
(A)Two state detachment process of the bead. (B) The bi-modal velocities of the bead under 5 pN applied load. (C) Measured stiffnesses of single kinesin and two kinesin assemblies. (D) Attenuated cargo size displacements.
Taken from: Jamison *et al*, Biophysical Journal 99, 2967, 2010.

Systematic analysis evinced the motors step asynchronously during cargo transport as a result of which attenuated cargo size displacements are observed.[44] To understand the system dynamics the cargo velocities of the two motors complex were measured. Owing to compliance in the behavior of kinesin-1 motor the compliance corrected version of the cargo velocities of the two motors system reveal that the system behaves like a single motor system below stalling force of kinesin-1 and there is a cooperative effect in the cargo velocities under loads greater than the single kinesin-1 stall force. The motors tend to cooperate under high forces yielding higher cargo velocities (Fig 2.5).
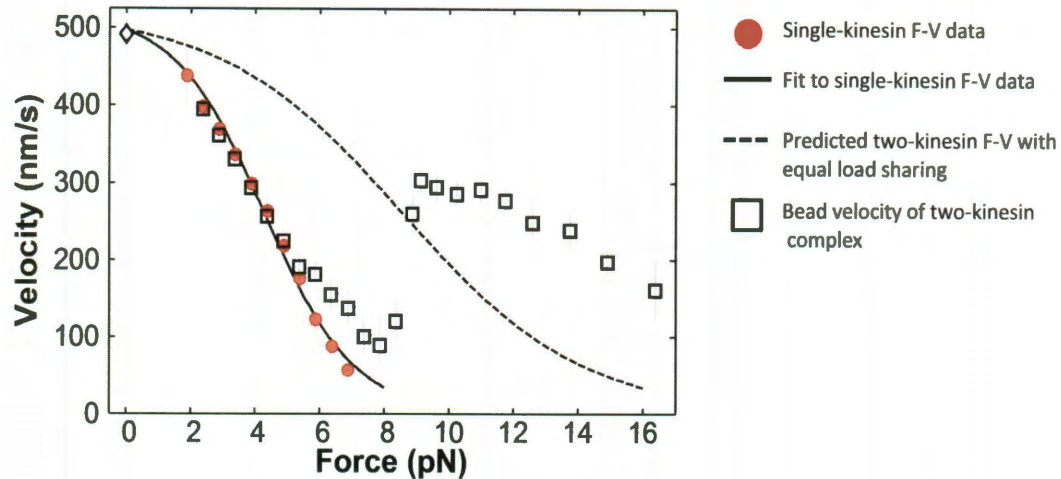
Figure 2.5 – Compliance corrected FV plot of the two motors complex.
Taken from: Jamison *et al*, Biophysical Journal 99, 2967, 2010.

To understand the dynamics of transport a theoretical model was constructed from single motor measurements. The model is essentially a discrete-state stochastic model that considers transitions occurring in the system from one microstate to another via configurations in mechanical equilibrium. So, the net force and torque acting on the system in such enumerated microstate configurations is balanced. The point of attachment of the motor to the MT and the position of the bead relative to the trap center under mechanical equilibrium defines a microstate configuration.

The free energy of the system in such a state is the sum total of the energy stored in the motor-bead linkage and the energy of the interaction between the bead and the trap. The key dynamical events that constitute cargo transport are stepping (forward, backward), binding and unbinding. The details of modeling these dynamical events and calculating the microstate energies of the complex are

discussed in detail in J.Driver *et al.*[46] To account for the work done by the motor against directional loads the model assumes a specific pathway along the motor's direction of stepping described in Fisher *et al.*[47]

The system dynamics is studied by numerically solving a set of Master equations which can be written down in a compact form: $\frac{d\psi}{dt} = \hat{A}\,\psi$. The transition rate matrix, $\hat{A}$ contains information about the rates of all possible transitions between the microstates and ψ represents all the microstates enumerated is written as a column vector. The stepping, binding and unbinding rates of transition are dependent on the difference in energies of the discrete microstates involved in the transition. Detailed balance principle is valid between the forward and backward stepping rates, and likewise between the binding and unbinding rates. The dynamics of the system is studied by enumerating the significant microstates and calculating their probability distributions at all times until the system reaches a steady state distribution. The calculated cargo velocities in static trapping and force-clamped treatments are compared against the measured values.

The Master equations can be written formally as shown below, and are subject to change with respect to microstate stepping transition (u and w) rates when the free energy profile pertinent to a stepping transition is modified.

Equation 2.1 Model master equations

$$\frac{d\psi^0}{dt} = \sum_i k_i^{\text{off}}\, \psi_i^a + \sum_j k_j^{\text{off}}\, \psi_j^b$$

$$\frac{d\psi_i^a}{dt} = u_{(i-1)\to i}\, \psi_{(i-1)}^a + w_{(i+1)\to i}\, \psi_{(i+1)}^a$$

$$-\left(k_i^{\text{off}} + \sum_j k_{i\to(i,j)}^{\text{on}} + u_{i\to(i+1)} + w_{i\to(i-1)} \right)\psi_i^a + \sum_j k_{(i,j)\to i}^{\text{off}}\, \psi_{(i,j)}^{a,b}$$

$$\frac{d\psi_i^a}{dt} = u_{(i-1)\to i}\, \psi_{(i-1)}^a + w_{(i+1)\to i}\, \psi_{(i+1)}^a$$

$$-\left(k_i^{\text{off}} + \sum_j k_{i\to(i,j)}^{\text{on}} + u_{i\to(i+1)} + w_{i\to(i-1)} \right)\psi_i^a + \sum_j k_{(i,j)\to i}^{\text{off}}\, \psi_{(i,j)}^{a,b}$$

$$\frac{d\psi_{(i,j)}^{a,b}}{dt} = \left(k_{i\to(i,j)}^{\text{on}}\, \psi_i^a + k_{j\to(i,j)}^{\text{on}}\, \psi_j^b \right) + u_{(i-1,j)\to(i,j)}\psi_{(i-1,j)}^{a,b} + u_{(i,j-1)\to(i,j)}\, \psi_{(i,j-1)}^{a,b}$$

$$+ w_{(i+1,j)\to(i,j)}\, \psi_{(i+1,j)}^{a,b} + w_{(i,j+1)\to(i,j)}\, \psi_{(i,j+1)}^{a,b}$$

$$- \left[k_{(i,j)\to i}^{\text{off}} + k_{(i,j)\to j}^{\text{off}} + u_{(i,j)\to(i+1,j)} + u_{(i,j)\to(i,j+1)} + w_{(i,j)\to(i-1,j)} \right.$$

$$\left. + w_{(i,j)\to(i,j-1)} \right] \psi_{(i,j)}^{a,b}$$

Here ψ is the probability of a microstate. The complex detached from the MT is represented as ψ^0, single motor bound states are represented as ψ^a or ψ^b and two motor bound states as $\psi^{a,b}$. The subscript labels i and j denote the microtubule lattice-site position of the motors. The labels i and j are used for microstate transition rates for motor binding (k^{on}), detachment (k^{off}), and stepping (u and w) to indicate the initial and final microstates of the system for that transition.

The earlier model predicts the motors cooperate negatively under low applied loads, where as the model predictions do not explain the high cargo velocities under high applied loads (Fig 2.6) and it has been suggested that locally interacting motors could coordinate their stepping behavior leading to positive cooperative effects under high applied loads from previous experimental analysis of bead size displacements.
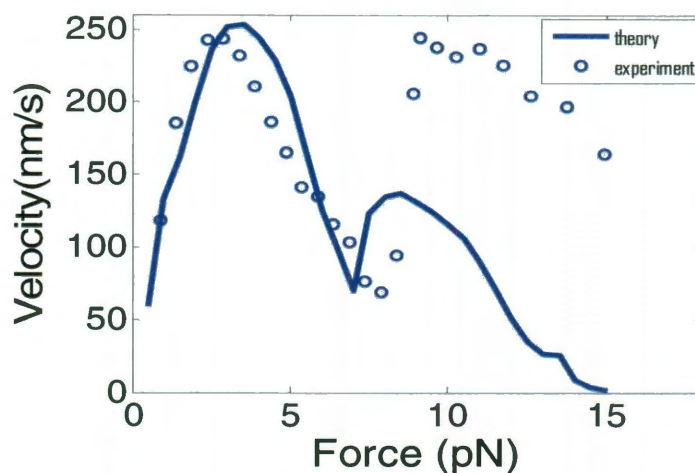
Figure 2.6 – Bead velocities of the two motors complex.
Circles represent measured bead velocities in the static optical trap and the solid blue line is the calculated bead velocity for the two kinesin system in a static optical trap.

Measurements of cargo velocities are higher than responses by the model and there is a need to incorporate cooperative affects into the current modeling framework. The cargo motion occurs via configurations of both single motor states and two motor bound states. The effect of coupling between the motors in the two motor

bound states when motors are closely spaced on the MT is incorporated into the

model to validate the cargo velocities under high applied loads.

Chapter 3

Cooperative interactions between motors affect dynamics of the complex

We have developed a model that incorporates interactions explicitly in the system. When the motors are closely located on the microtubules the energy barriers of the transition states for motor stepping transitions are lowered, by introducing a multiplicative factor in the expressions of stepping rates (without violating detailed balance principle). With the multiplicative/enhancement factor in the stepping rate expressions included and upon solving the Master equations, the computed cargo velocities were compared with the measured values. The model also considered the effect of local deformations due to closely spaced motors on cargo velocities. It has been reported earlier that MT structures can undergo mechanical deformations when subject to loads. Motors bound to the MT binding sites interact with these structures by exerting forces on them. When the motors are nearby they could experience each other's interaction potential with the microtubules thus affecting the free energy profile of the motors.
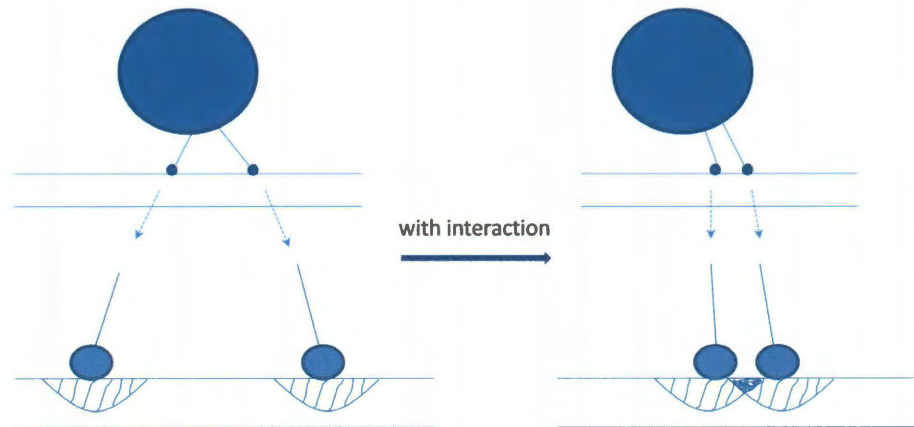
Figure 3.1 – Schematic of interactions between closely spaced motors on microtubules.
The schematic depicts the motors separated far apart on the left, and closely spaced on the microtubules on the right.

Due to the deformations caused by loads exerted by the motors on the microtubule, a closely spaced motor (≤16.4nm) can experience the microtubule lattice shorten, due to which a proportionate displacement could be transcribed to the complex. This allows the transitioning motor to perform work under assisting load, due to which the free energy profile is modified thus paving way for the motor to perform less work during sub-step transitions and transition with higher stepping rates. The cargo velocities were computed for distinct motor stepping pathways. In this approach the transition state and intermediate state positions of the reaction coordinate are affected in a distance dependent manner. However, dynamic properties of the complex are dependent on geometry on the MT, and henceforth depend on how the loads are distributed between the motors at any

given applied load. The cargo velocities were computed for stepping pathways considering the transition state motions as a function of load experienced by the motor, since motions of the transition states under high loads should undergo more displacement than under low loads. Our calculations using both the methodologies in static and force-feedback modes helped us to analyze the system dynamics and put forth a mechanism for molecular transport.

Motivated by measurements of cargo velocities pertinent to coupled motors transport under high applied loads the role of local interactions affecting dynamic properties of the cargo is considered. Although the earlier model predictions for cargo velocities are in good agreement under low applied loads and the bi-modal nature of the Force-Velocity curve is evinced, a good agreement under high applied loads was lacking. To explicate reasons for this behavior the transition state energy barriers were lowered thereby increasing the stepping rates owing to an enhancement factor of 4.0 under the condition that the interacting motors on the MT are within 16.4 nm separation distance. An enhancement factor of 4.0 implicates lowering of the transition state barriers approximately by $1.38k_BT$ pertinent to a microstate transition. As a result of affecting the stepping rates by an enhancement factor, in the static trap case a slight increase in cargo velocities can be noted under low applied loads indicating the presence of two motor states and the cargo velocities become appreciably higher under high applied loads with the complex stalling at around 15 pN applied load. The impact of the enhancement factor in the low force region of force-feedback calculations is more than the static trap case since the density of two motor states is higher in the force-feedback mode compared

to the static mode scenario. Also the affect of different unloaded (k^{on}-1/s to 5/s in integer steps) binding rates is considered to calculate the FV plots. The FV plot in the black (Fig 3.2) corresponds to an unloaded binding rate constant of 1/s. A lower unloaded binding rate constant leads to a drop in the cargo velocities in the low force region.
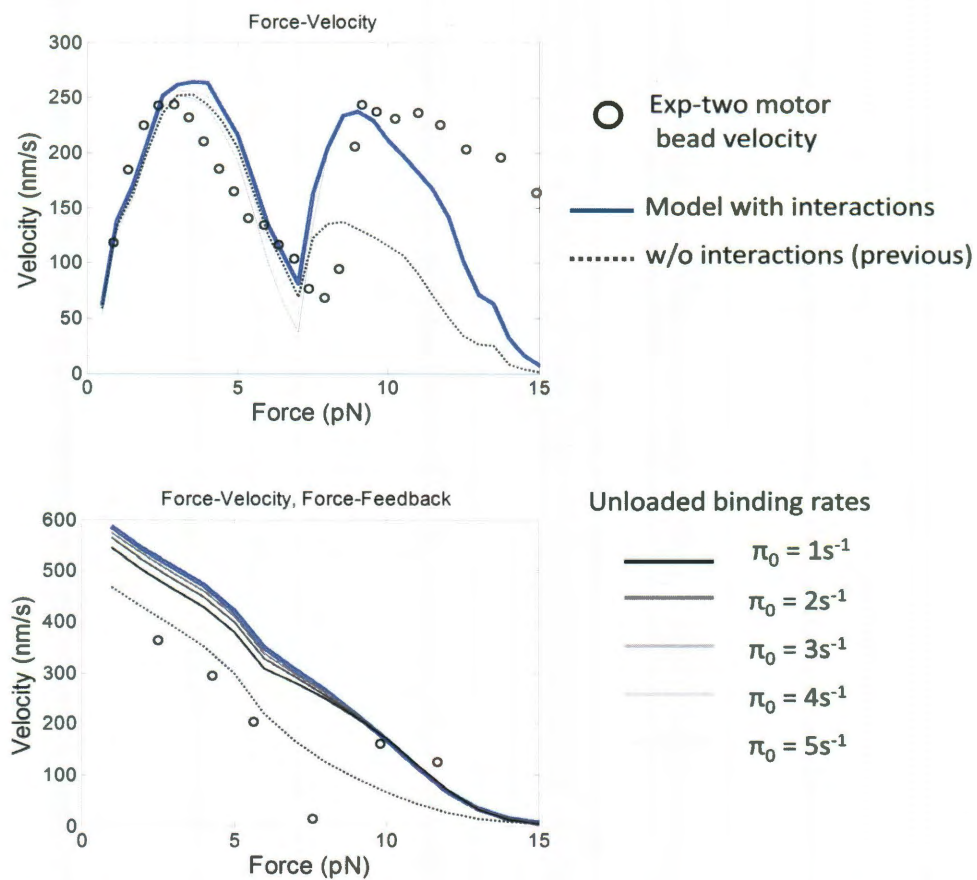
Figure 3.2 – Enhancement factor dependent interactions and cargo velocities. The FV plot in the static trap (top) and force (bottom) feedback.

While probing for a molecular mechanism, the distance dependent motion of the transition states in the motor's stepping pathway allowed the motor to perform less

work thus aiding higher stepping rates of transition in order to achieve the 8.2 nm step size. Applying a change to the x-direction of motion for transition states in the reaction coordinate elucidated by Fisher *et al*, the phenomenological reaction coordinate of TS_1:-0.78nm, IS: -0.05nm, TS_2: -3nm relative to the binding position of the motor explicates the measured data the best in the static trap case.[47] Also the effect of different unloaded binding rates on the calculated cargo velocities show some decrease near the stalling force ($\sim$ 7pN) of single kinesin-1 motor. Whereas in the case of force-clamped calculations, an unusual increase in the cargo velocity near the stalling force was noted.
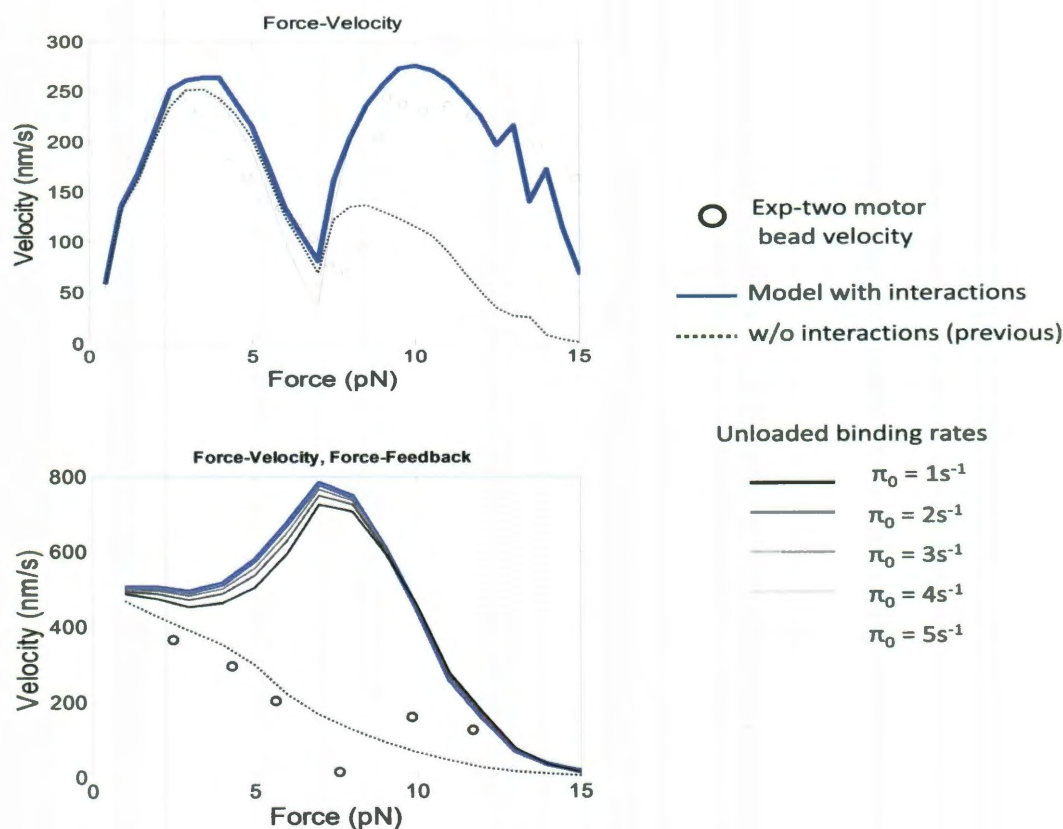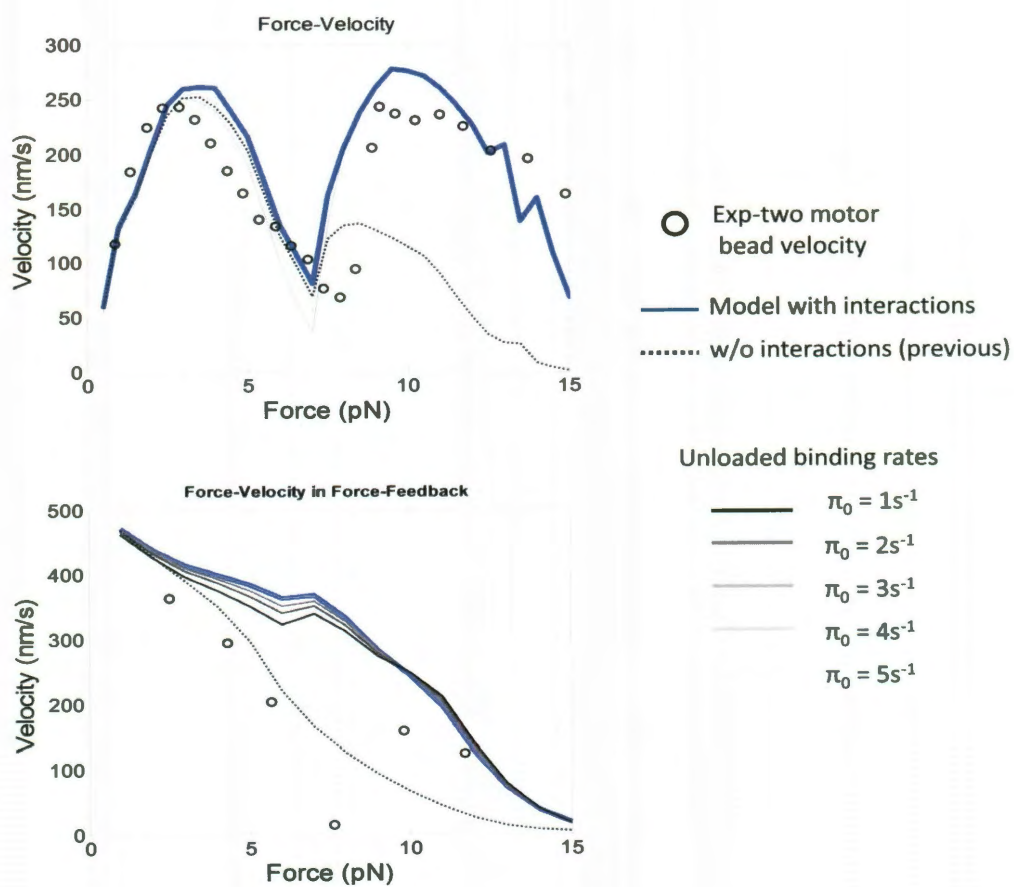

Figure 3.3 – Distance dependent interactions and cargo velocities.
The FV plot in the static trap (top) and force (bottom) feedback.

This clearly contradicts the nature of Force-Velocity relationship seen in experiments. The unexpected cargo velocities in force-feedback calculations are due to the drastic increase in the kinesin-1 motor velocities along the modified stepping pathway and the density of states in force-feedback being higher than those in the static trap case. Hence this approach did not concur with the measurements in force-feedback mode. When the motions of the transition states are parameterized as a function of the force felt by the transitioning motor, we observe agreeable results in both static and force-feedback calculations. The forces that the motors exert on the microtubules compressing the structure locally, causing a displacement of the complex, justifies the parameterization of the motions of transition states in terms of force experienced by the transitioning motor. In the treatment of force dependent motion of transition states we assume stiffness of microtubules to be approx 2.3 pN/nm. In our treatment, under zero applied load the position of TS_1 is same as that of the original reaction coordinate, likewise for the IS and the TS_2 position. At the stalling force of the kinesin-1 motor the positions of TS_1, IS and TS_2 are moved to -0.78, -0.05, -3.0 nm respectively. Motors interacting locally cause the microtubule lattice size to shorten. This shift has been imbibed into the reaction coordinate of the motor stepping pathway, but in a force-dependent way. Thus, the calculated FV plots employing this methodology in static and feedback modes validated the measured data fairly well. The effect of unloaded binding rates (k^{on} = 1/s to 5/s in integer steps) in the calculations evinces the appearance of the FV relationship in force-feedback experiments. The measurements in the force-

feedback mode are best explicated when the transition states are affected in a force

dependent manner and when the unloaded binding rate constant of 1/s.

Figure 3.4 – Force dependent interactions and cargo velocities.
The FV plot in the static trap (top) and force (bottom) feedback.

In conclusion, we presented an extended model that incorporates the role of interactions in the system. A molecular mechanism was probed using interactions to explicate the cargo velocities via parameterization of the motion of transition states of the motor along the reaction coordinate. Owing to local interactions in between motors and microtubule, the motions of the transition states along the motor's reaction coordinate are affected by the forces that the motors experience. Transcribing the force dependent feature for transition state motions into the reaction coordinate for the motor yields agreeable results in the static and force-feedback modes. The rationale that the stepping rates are affected with motor microtubule interactions can be understood when these results are compared with those of the calculated FV plots employing an enhancement factor in front of the stepping rate expressions in which case the free energy barriers of the transitions are lowered.

References

1) Howard, J. *Mechanics of Motor Proteins and the Cytoskeleton*; Sinauer Associates: Sunderland, MA, 2001.

2) Vale, R. D. The molecular motor toolbox for intracellular transport. *Cell*, **2003**, *112*, 467.

3) Berry RM, Armitage JP. The bacterial flagella motor. *Adv.Microb.Phys*, **1999**, *41*, 292.

4) Elston TC, Oster, G. Protein turbines I: the bacterial flagellar motor. *Biophys. J*, **1997**, *73*, 703.

5) Sowa Y, Rowe AD, Leake MC, Yakushi T, Homma M et al. Direct observation of steps in rotation of the bacterial flagellar motor. *Nature*, **2005**, *437*, 916.

6) Rondelez Y, Tresset G, Nakashima T, Kato-Yamada Y, Fujita H et al. Highly coupled ATP synthesis by F_1-ATPase single molecules. *Nature*, **2005**, *433*, 774.

7) Rice S, Lin AW, Safer D, Hart CL, Naber N et al. A structural change in the kinesin motor protein that drives motility. *Nature*, **1999**, *402*, 778.

8) De La Cruz EM, Wells AL, Rosenfeld SS, Ostap EM, Sweeney HL. The kinetic mechanism of myosin V. *PNAS*, **1999**, *96*, 13726.

9) Mehta AD, Rock RS, Rief M, Spudich JA, Mooseker MS, Cheney RE. Myosin-V is a processive actin-based motor. *Nature*, **1999**, *400*, 590.

10) Schnitzer MJ, Visscher K, Block SM. Force production by single kinesin motors. *Nat.Cell.Biol*, **2000**, *2*, 718.

11) Mehta A. Myosin learns to walk. *J.Cell.Sci*, **2001**, *114*, 1981.

12) Asbury CL, Fehr AN, Block SM. Kinesin moves by an asymmetric hand-over-hand mechanism. *Science*, **2003**, *302*, 2130.

13) Yildiz A, Tomishige M, Vale RD, Selvin PR. Kinesin walks hand-over-hand. *Science*, **2003**, *302*, 676.

14) Schnitzer MJ, Block SM. Kinesin hydrolyzes one ATP per 8-nm step. *Nature*, **1997**, *388*, 386.

15) Gilber SP, Sloboda, RD. Bidirectional transport of fluorescently labeled vesicles introduced into extruded axoplasm of squid loligo pealei. *J.Cell Biol*, **1984**, *99*, 445.

16) Rogers SL, Tint IS, Fanapour PC, Gelfand VI. Regulated bidirectional motility of melanophore pigment granules along microtubules *in vitro*. *PNAS*, **1997**, *94*, 3720.

17) Vale RD, Malik F, Brown D. Directional instability of microtubule transport in the presence of kinesin and dynein, two opposite polarity microtubule motor proteins. *J.Cell Biol*, **1992**, *119*, 1589.

18) Visscher K, Schnitzer MJ, Block SM. Single kinesin molecules studied with a molecular force clamp. *Nature*, **1999**, *400*, 184.

19) Block SM, Asbury CL, Shaevitz JW, Lang MJ. Probing the kinesin reaction cycle with a 2D optical force clamp. *PNAS*, **2003**, *100*, 2351.

20) Strick TR, Allemand JF, Bensimon D. Stress-induced structural transitions in DNA and proteins. *Annu.Rev.Biophys.Biomol.Struct*, **2000**, *29*, 523.

21) Charvin G, Bensimon D, Croquette V. Single-molecule study of DNA unlinking by eukaryotic and prokaryotic type-II topomerases. *PNAS*, **2003**, *100*, 9820.

22) Itoh H, Takahashi A, Adachi K, Noji H, Yashuda R, et al. Mechanically driven ATP synthesis by F_1-ATPase. *Nature*, **2004**, *427*, 465.

23) Snyder GE, Sakamoto T, Hammer JA, Sellers JR, Selvin PR. Nanometer localization of single green fluorescent proteins: evidence that myosin V walks hand-over-hand via telemark configuration. *Biophys.J*, **2004**, *87*, 1776.

24) Yildiz A, Park H, Safer D, Yang Z, Chen LQ, et al. Myosin VI steps via a hand-over-hand mechanism with its lever arm undergoing fluctuations when attached to actin. *J.Biol.Chem*, **2004**, *279*, 37223.

25) Higushi H, Muto E, Inoue Y, Yanagida T. Kinetics of force generation by single kinesin molecules activated by laser photolysis of caged ATP. *PNAS*, **1997**, *94*, 4395.

26) Block SM. Making light work with optical tweezers. *Nature*, **1992**, *360*, 493.

27) Ally S, Larson AG, Barlan K, Rice SE, Gelfand VI. Opposite-polarity motors activate one another to trigger cargo transport in live cells. *J.Cell.Biol*, **2009**, *187*, 1071.

28) Kulic IM, Brown AE, Kim H, Kural C, Blehm B, Selvin PR, Nelson PC, Gelfand VI. The role of microtubule movement in bidirectional organelle transport. *PNAS*, **2008**, *105*, 10011.

29) Holzbaur EL, Goldman YE. Coordination of molecular motors: from in vitro assays to intracellular dynamics. *Curr.Opin.Cell.Biol*, **2010**, *22*, 4.

30) Klumpp S, Lipowsky R. Cooperative cargo transport by several molecular motors. *PNAS*, **2005**, *102*, 17284.

31) Ori-McKenney KM, Xu J, Gross SP, Vallee RB. A cytoplasmic dynein tail mutation impairs motor processivity. *Nat.Cell.Biol*, **2010**, *12*, 1228.

32) Hendricks AG, Perlson E, Ross JL, Schroeder HW, Tokito M, Holzbaur EL. Motor coordination via a tug-of-war mechanism drives bidirectional vesicle transport. *Curr.Biology*, **2010**, *20*, 697.

33) Soppina V, Rai AK, Ramaiya AJ, Barak P, Mallik R. Tug-of-war between dissimilar teams of microtubule motors regulates transport and fission of endosomes. *PNAS*, **2009**, *106*, 19381.

34) Julicher F, Ajdari A, Prost J. Modeling molecular motors. *Rev.Mod.Phys*, **1997**, *69*, 1269.

35) Kolomeisky AB, Widom B. A simplified "ratchet" model of molecular motors. *J.Stat.Phys*, **1998**, *93*, 633.

36) Fisher ME, Kolomeisky AB. The force exerted by a molecular motor. *PNAS*, **1999**, *96*, 6597.

37) Fisher ME, Kolomeisky AB. Molecular motors and the forces they exert. *Phys. A*, **1999**, *274*, 241.

38) Lipowsky R. Universal aspects of the chemomechanical coupling for molecular motors. *PRL*, **2000**, *85*, 4401.

39) Bustamante C, Keller D, Oster G. The physics of molecular motors. *Acc.Chem.Res*, **2001**, *34*, 412.

40) Ali MY, Lu H, Bookwalter CS, Warshaw DM, Trybus KM. Myosin V and kinesin act as tethers to enhance each others' processivity. *PNAS*, **2008**, *105*, 4691.

41) Leduc C, Ruhnow F, Howard J, Dietz S. Detection of fractional steps in cargo movements by the collective operation of kinesin-1 motors. *PNAS*, **2007**, *104*, 10847.

42) Barbero P, Bittova L, Pfeffer SR. Visualization of Rab9-mediated vesicle transport from endosomes to trans-Golgi in living cells. *Journal of Cell Biology*, **2002**, *156*, 511

43) Rogers AR, Driver W, Constantinou PE, Jamison DK, Diehl MR. Negative interference dominates collective transport of kinesin motors in the absence of load. *PCCP*, **2009**, *11*, 4882.

44) Jamison DK, Driver JW, Rogers AR, Constantinou PE, Diehl, M. R. Two kinesins transport cargo primarily via the action of one motor: implications for intracellular transport. *Biophys Journal*, **2010**, *99*, 2967.

45) Korn C, Klumpp S, Lipowsky R, Schwarz US. Stochastic simulations of cargo transport by processive molecular motors. *J.Chem.Phys*, **2009**, *131*, 245107.

46) Driver JW, Jamison DK, Uppulury K, Rogers AR, Kolomeisky AB, Diehl MR. Productive cooperation among processive motors depends inversely on their mechanochemical efficiency. *Biophys. Journal*, **2011**, *101*, 386.

47) Fisher ME, Kim YC. Kinesin croches to sprint but resists pushing. *PNAS*, **2005**, *102*, 16209.

48) Schaap IAT, Carrasco C, de Pablo PJ, MacKintosh FC, Schmidt CF. Elastic response, buckling and instability of microtubules under radial indentation. *Biophys. Journal*, **2006**, *91*, 1521.

49) Gittes F, Mickey B, Nettleton J, Howard J. Flexural rigidity of microtubules and actin filaments measured from thermal fluctuations in shape. *Journal of Cell Biology*, **1993**, *120*, 923.

50) Kolomeisky AB, Fisher ME. Molecular motors: A theorist's perspective. *Annual reviews of Phys.Chemistry*, **2007**, *58*, 675.